www.springer.com/41230
https://doi.org/10.1007/s41230-025-4204-0
Research & Development
Vol. 22 No. 5 September 2025
CHINA FOUNDRY

Vat photopolymerization 3D printing of Al_2O_3 ceramic cores with TPMS micro lattice structure

Xiao-fei Zhai[1, 2], Jing-yi Chen[2], Xue-qin Zhang[2], Yuan-hong Qian[1], Rong Chen[1], Wei Zhang[1], and *Ru-jie He[2]

1. Aerospace Additive Technology (Beijing) Co., Ltd., Beijing 100071, China

2. Institute of Advanced Structure Technology, Beijing Institute of Technology, Beijing 100081, China

Abstract: The complex ceramic core used for hollow turbine blades requires a high porosity and a high flexural strength. For a better balance between porosity and flexural strength, ceramic materials with porous structures are preferred. In order to achieve the transition from disordered pore formation to ordered pore formation, Al_2O_3 ceramic cores with triply periodic minimal surface (TPMS) micro lattice structures with different structural configurations (gyroid, diamond, and neovius) and different volume fractions of lattice structures (30, 40, and 50, vol.%) were designed and prepared by vat photopolymerization 3D printing. The effects of structural configuration and volume fraction of the lattice structure on the following structural shrinkage, microstructure, and flexural strength were investigated. The shrinkage relationship of the three lattice configurations is: neovius>diamond>gyroid. Besides, it is found that with an increase in the volume fraction of the 3D printed Al_2O_3 ceramic micro lattice structures, their flexural strength correspondingly increases ranging from 54.95 MPa to 139.1 MPa. The maximum average flexural strength of the 3D printed Al_2O_3 ceramic micro lattice structures is obtained when the structural configuration is diamond and with a volume fraction of 50vol.%, which is 139.1 MPa. Even when the volume fraction of the lattice structure is 30vol.%, that is to say the porosity is 70%, the flexural strength is as high as 50–70 MPa, which can still be maintained at a high level. In addition, when the volume fraction of the lattice structure is a certain value, the sample with diamond configuration has a higher strength. The internal pore morphology, pore size, and porosity of the cores are precisely controlled, achieving both a high porosity and a high strength. Therefore, this study maintains high porosity and high strength simultaneously, providing a new lattice structure design idea for 3D printed ceramic cores.

Keywords: alumina ceramic cores; vat photopolymerization 3D printing; micro lattice; microstructure; mechanical property

CLC numbers: TG221 **Document code:** A **Article ID:** 1672-6421(2025)05-565-09

1 Introduction

Ceramic cores are mainly used for investment casting of complex cavity structures in aircraft engine blades [1]. As the aviation industry's need for engines with a higher thrust-to-weight ratio continues to grow, the shape and structure of ceramic cores are becoming increasingly complex, which poses strict requirements for their precision forming [2-4]. Traditional forming methods cannot achieve high-precision manufacturing of complex shaped ceramic cores [5-7]. 3D printing technology (also known as additive manufacturing) can break through traditional technological bottlenecks and achieve high-precision and rapid formation of complex shaped ceramic cores [8-10].

As is known, the ceramic cores need to be removed after casting. At present, the removal of ceramic cores in industrial production is mostly carried out by boiling alkali method, which involves the reaction of strong alkali solution with alumina under high temperatures and high pressures to cause the cores to collapse [11, 12]. The efficiency of de-coring is closely related to the porosity of the cores. An increase in porosity can increase the contact area between alkaline solution and alumina matrix, and improve the efficiency of core removal. Some studies focus on preparing porous ceramics by improving sintering processes to increase the porosity of Al_2O_3 ceramic cores [13, 14]. Li et al. [15] prepared the green body of Al_2O_3 ceramic cores using vat photopolymerization 3D printing technology, and

*Ru-jie He

Male, Ph. D., Professor. His research interests mainly focus on additive manufacturing of ceramics and ceramic matrix composites.

E-mail: herujie@bit.edu.cn

Received: 2024-10-02; Revised: 2024-11-25; Accepted: 2025-01-12

obtained the porosity of the Al_2O_3 ceramic cores of 33.8% and 37.9% after sintering at 1,350 °C and 1,150 °C, respectively. Ceramic cores need to have a certain strength to resist the impact of molten metal during the casting process [18]. Usually, the porosity of ceramics sintered at low temperatures can be increased, but it is always accompanied by a rapid decrease in strength [16, 17]. It is not reasonable to only focus on the porosity but ignore the strength loss of the ceramic cores. Porosity and strength, as two variables that constrain each other, existing balancing strategies of 3D printed Al_2O_3 ceramic cores are still insufficient to address the key technical challenge of the mutual constraints. Therefore, it is deem necessary to achieve a high porosity and a high strength simultaneously of the 3D printed Al_2O_3 ceramic cores.

Structural design is a promising approach to 3D printed ceramic cores with simultaneously a high strength and a high porosity [10]. One of the major advantages of 3D printed ceramics is that they are not limited by molds and can be formed into complex structures. Interestingly, the use of 3D printing technology to prepare micro lattice structures has been applied in fields such as catalysts and lattice scaffolds [19]. Wang et al. [20] used vat photopolymerization 3D printing to prepare polymer microcrystals with micro/nano lattice structures, which exhibited superior compressive strength compared to existing micro/nano materials and bulk materials. Zhang et al. [21] also used vat photopolymerization 3D printing to prepare micro/submicron sized microcrystalline lattice scaffolds using acrylic resin as the raw material, and achieved excellent mechanical properties. Feng et al. [22] prepared SiOC ceramics with a lattice structure based on 3D printing technology, achieving adjustable shape and controllable thickness, and exhibiting good mechanical performance. All these works prove that 3D printed micro lattice structures have the potential to obtain both a high porosity and a high strength at the same time. Therefore, it has good reason to believe 3D printed ceramic cores with micro a lattice structure is a good method to meet high porosity and high strength at the same time. At present, however, there is a lack of ordered hole design methods in the field of 3D printed Al_2O_3 ceramic cores.

In this study, Al_2O_3 ceramic cores with triply periodic minimal surface (TPMS) micro lattice structures with different structural configurations (gyroid, diamond, and neovius) and different volume fractions of lattice structures (30, 40, and 50, vol.%) were designed and prepared using vat photopolymerization 3D printing. The effects of structural configurations and volume fractions of lattice structures on the following structural shrinkage, microstructure, and flexural strength were investigated. This study is believed to provide a new lattice structure design idea for simultaneously increasing the porosity and strength of 3D printed ceramic cores.

2 Experiment

2.1 Raw materials

The ceramic slurry used for the following vat photopolymerization 3D printing was mainly consisted of ceramic powders and photosensitive resin. Two kinds of particle sizes of Al_2O_3 particles (purity>99.9%, Zhongzhou Alloy Materials Co., Ltd., China) were used for particle grading, including coarse Al_2O_3 powder with a median diameter of 10.34 μm and fine Al_2O_3 powders with a median diameter of 1.05 μm. The photosensitive resin was a blend of 1,6-ethanediol diacrylate (HDDA, Changshu Hengrong Trading Co., Ltd., China) and trihydroxy methacrylate (TMPTA, Shanghai Aladdin Co., Ltd., China). TPO (Guangzhou Kangoushuang Trading Co., Ltd., China) was used as the photoinitiator and KOS110 (Guangzhou Kangoushuang Trading Co., Ltd., China) was used as the dispersant.

2.2 Fabrication and characterization of Al_2O_3 ceramic cores

The fabrication process of the Al_2O_3 ceramic cores with TPMS micro lattice structures included three steps: slurry preparation, vat photopolymerization 3D printing, and debinding and sintering.

(1) Slurry preparation

Al_2O_3 ceramic particles were added to HDDA/TMPTA (40vol.%/10vol.%) resin monomer, followed by the addition of TPO (based on 1vol.% of the total volume of HDDA and TMPTA) and KOS110 (based on 2vol.% of the total volume of alumina), and milled using ZrO_2 balls at 400 $r \cdot min^{-1}$ for 22 h to obtain a Al_2O_3 ceramic-resin slurry with a solid content of 50vol.%.

(2) Vat photopolymerization 3D printing

TPMS micro lattice structures with three different structural configurations: gyroid, diamond, and neovius were designed. All the designed models were drawn using Solidworks software (Solidworks, Dassault Systemes S.A., USA), saved as STL. format, imported into a 3D printing slicing software (S10, Beijing TenDimensions Technology Co., Ltd., China) for slicing, and the printing thickness was set to 50 μm. As shown in Fig. 1, the ceramic slurry was poured into the trough of the vat photopolymerization 3D printer (AUTOCERA-R, Beijing TenDimensional Technology Co., Ltd., China), and the thickness of the slurry was maintained at 100 μm. The wavelength of the laser was 405 nm, and the intensity of the light was set to 12,000 $\mu W \cdot cm^{-2}$. After 3D printing, the green bodies were ultrasonically cleaned in ethanol for 3 min to remove the residual slurry on the surface. In this study, the Al_2O_3 ceramic micro lattice green bodies for the following structural shrinkage measurement, porosity testing, and microstructural observation were designed as 10 mm×10 mm×10 mm, and the green bodies for the following flexural strength testing were designed as 6 mm×8 mm×40 mm.

(3) Debinding and sintering

Subsequently, debinding and sintering were carried out. The debinding was conducted in a furnace (FMJ-19/13, Hefei Facerom Furnace Co., Ltd., China) following steps as below: room temperature–250 °C: heating rate of 1 $°C \cdot min^{-1}$; 250 °C–550 °C: heating rate of 0.5 $°C \cdot min^{-1}$ and holding at 550 °C

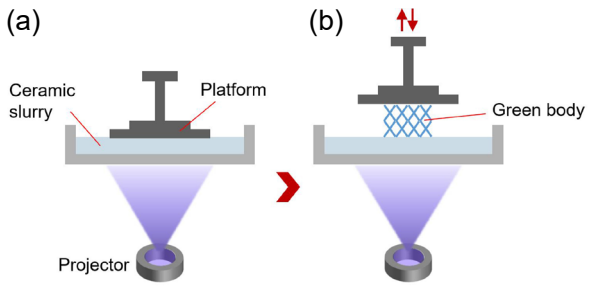

Fig. 1: Schematic diagram of vat photopolymerization 3D printing

for 2 h; 550 °C–800 °C: heating rate of 2 °C·min^{-1}; 800 °C^{-1}–1,000 °C: heating rate of 4 °C·min^{-1} and kept at 1,000 °C for 2 h. Then, the sample was cooled to room temperature and transferred to another furnace (FMJ-90/17, Hefei Facerom Furnace Co., Ltd., China) to complete the sintering process. The sintering process flow was: room temperature–1,000 °C: heating rate of 7.5 °C·min^{-1}; 1,000 °C–1,200 °C: heating rate of 5 °C·min^{-1} and holding at 1,200 °C for 30 min; 1,200 °C–1,650 °C: heating rate of 4 °C·min^{-1} and holding at 1,650 °C for 3 h; 1,650 °C–1,200 °C: cooling rate of 5 °C·min^{-1}. Finally, the sample was cooled to room temperature in the furnace to obtain the final Al_2O_3 ceramic sintered sample with a micro lattice.

In this work, 9 groups of Al_2O_3 ceramic micro lattice samples were prepared, as listed in Table 1. Three structural configurations with a cell length of 4 mm, including gyroid, diamond, and neovius, and three volume fractions of lattice structures: 30vol.%, 40vol.%, and 50vol.%, were designed. Correspondingly, the porosity of the samples is 70%, 60%, and 50%, respectively.

2.3 Characterization

The photos of the Al_2O_3 ceramic micro lattice green and sintered samples were taken by a digital camera (EOS 90D, Cannon, Japan). The microstructure of the Al_2O_3 ceramic micro lattice sintered samples was observed using a scanning electron microscope (SEM, JSM-7500F, Hitachi, Japan). The electron acceleration voltage during the SEM observation was 10 kV.

Referring to the HB5353.2-2004 industrial standard, the structural shrinkage (s) of the Al_2O_3 ceramic micro lattice sintered samples was measured and calculated. The dimensions of the sample in the x (length), y (width), and z (height) directions before and after sintering were measured and recorded by a vernier caliper (36-111-23, Stanley, USA). Each group was measured 5 times, and an average result was taken. The equation for defining the shrinkage rate was given as follows:

$$s_x = \frac{x_0 - x}{x_0} \times 100\% \quad (1)$$

$$s_y = \frac{y_0 - y}{y_0} \times 100\% \quad (2)$$

$$s_z = \frac{z_0 - z}{z_0} \times 100\% \quad (3)$$

s_x, s_y, s_z–Linear shrinkage (%) in the x, y, and z directions.

Table 1: Al_2O_3 ceramic micro lattice samples prepared in this work

Structural configuration	Labels	Volume fraction of lattice structure (vol.%)
Gyroid	Gyroid-30	30
	Gyroid-40	40
	Gyroid-50	50
Diamond	Diamond-30	30
	Diamond-40	40
	Diamond-50	50
Neovius	Neovius-30	30
	Neovius-40	40
	Neovius-50	50

x_0, y_0, z_0–The length (mm) of the green body in the x, y, and z directions.

x, y, z–The length (mm) of the sintered body in the x, y, and z directions.

An universal testing machine (LEGEND 2367, Instron Corporation, USA) was used to test the three-point flexural strength of the sintered sample. The test temperature was 25 °C, the loading rate was 0.5 mm·min^{-1}, and the span was 30 mm. At least five samples were tested for each condition to get the average value and minimize testing error.

3 Results and discussion

3.1 Microstructure and shrinkage

The photos of the green and sintered bodies structure of the as-prepared Al_2O_3 ceramic micro lattice are shown in Fig. 2, demonstrating good formability. Figure 3 shows the SEM images of Al_2O_3 ceramic micro lattice sintered samples with gyroid configuration at three volume fractions of 30vol.%, 40vol.%, and 50vol.%. The characteristic of the TPMS structure is that the average curvature of the surface is zero, and the overall structure constantly changes. From the enlarged partial view, obvious layering phenomenon can be observed, which is due to the imperfect matching between the printing layer thickness and the single-layer curing thickness during the 3D printing process, resulting in a "step" effect and a decrease in printing accuracy. However, the structure as a whole is free of defects such as porosity and cracks and is structurally intact. As can be seen in the partial enlargement of the bottom surface, the edges of the printed layer are sharply defined and free of defects. In addition, as the volume fraction of the lattice structure increases, the overall structure of the gyroid configuration remains unchanged, with a decrease in pore size and an increase in wall thickness, and all pores are connected. Since ceramic cores need to be de-cored after casting, TPMS configurations with connecting holes can greatly improve de-coring efficiency.

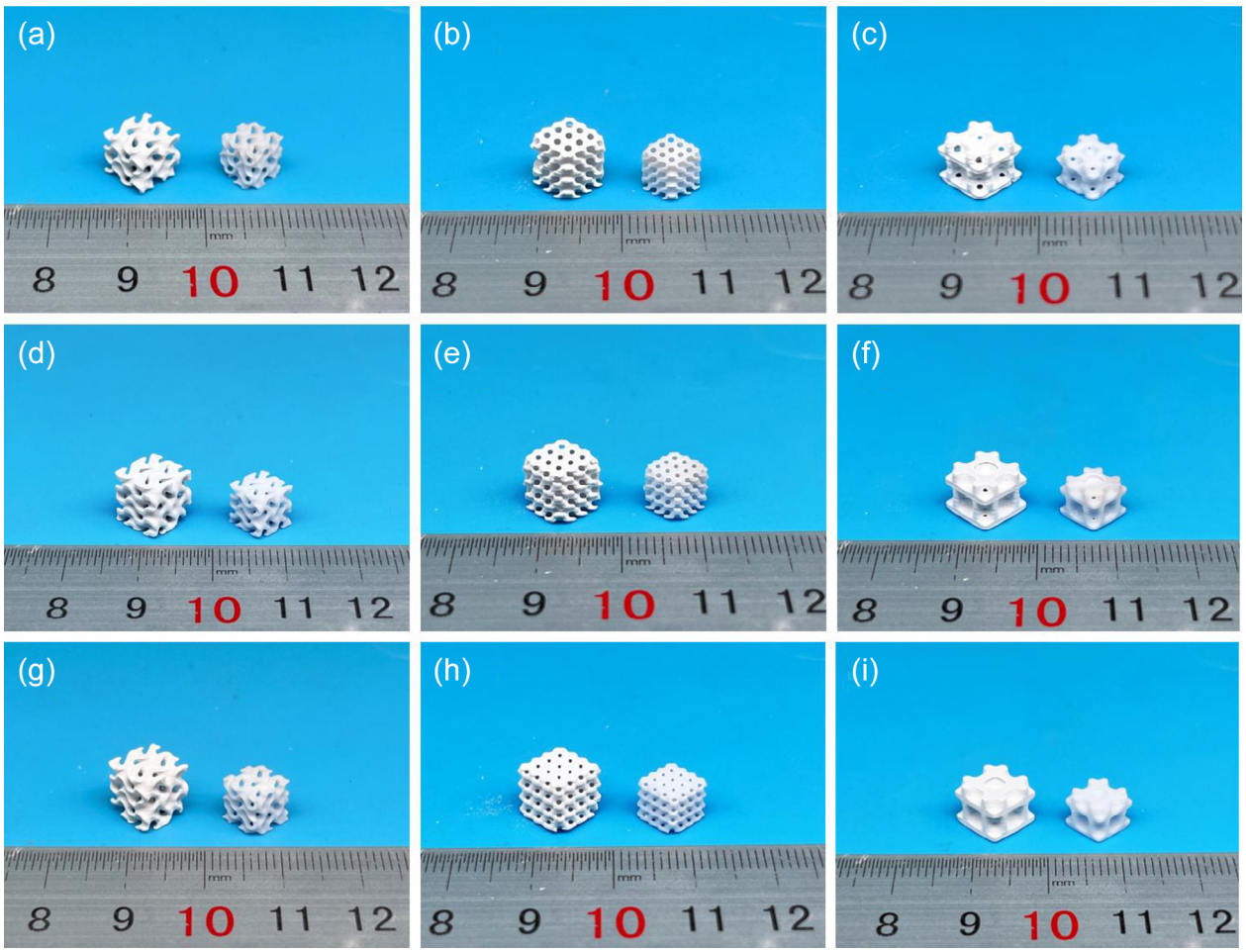

Fig. 2: Green and sintered 3D printed Al_2O_3 ceramic samples with a micro lattice structure: (a) gyroid-30; (b) diamond-30; (c) neovius-30; (d) gyroid-40; (e) diamond-40; (f) neovius-40; (g) gyroid-50; (h) diamond-50; (i) neovius-50. (In all photos, the left side is the 3D printed green body, and the right side is the sintered sample)

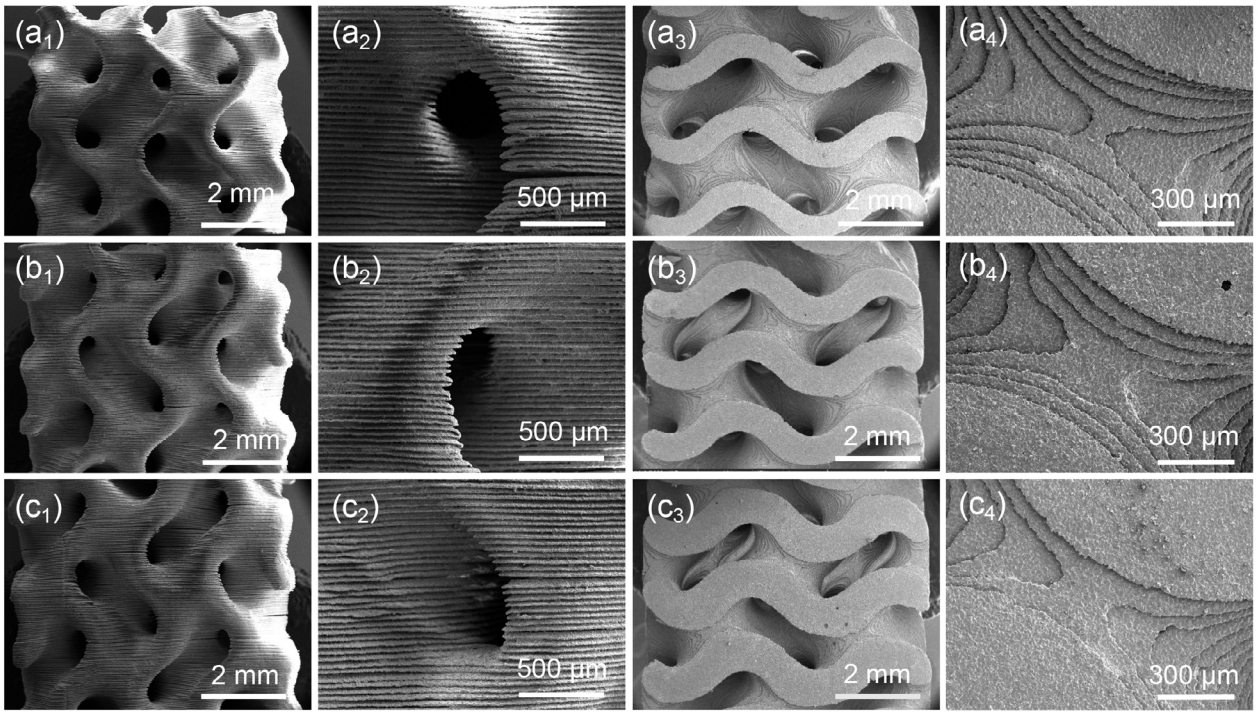

Fig. 3: SEM images of the Al_2O_3 ceramic micro lattice sintered bodies with gyroid configuration: (a_1, a_2) the side surface of gyroid-30; (a_3, a_4) the bottom surface of gyroid-30; (b_1, b_2) the side surface of gyroid-40; (b_3, b_4) the bottom surface of gyroid-40; (c_1, c_2) the side surface of gyroid-50; (c_3, c_4) the bottom surface of gyroid-50

Figure 4 shows the SEM images of Al_2O_3 ceramic micro lattice sintered samples with diamond configuration at three volume fractions of 30vol.%, 40vol.%, and 50vol.%. Compared to the samples with gyroid configuration, the samples with diamond configuration has a smaller pore size and thinner wall thickness. With the increase of the volume fraction of the lattice structure, the connected portion of the sample with diamond configuration increases, and adjacent surfaces gradually contact each other and form pores, while the wall thickness increases. The bottom surface pores of the samples with diamond configuration are approximately circular, with a decreasing pore size as the volume fraction of the lattice structure increases. Due to the special properties of TPMS with diamond configuration, the internal pore sizes are constantly changing: the bottom pore size is approximately 1,000 μm at the volume fraction of 30vol.%, 900 μm at 40vol.%, and 800 μm at 50vol.%. The pore size decreases with increasing volume fraction of the lattice structure, and at different volume fractions of lattice structures, all pores in the diamond configuration are connected, as observed by SEM.

Figure 5 shows the SEM images of the Al_2O_3 ceramic micro lattice sintered bodies with diamond configuration at three volume fractions of 30vol.%, 40vol.%, and 50vol.%. Compared to the samples with gyroid and diamond configurations, the samples with neovius configuration show significant printing defects. The printed interlayer phenomenon can be seen clearly in the SEM image of the side surface, with cracks appearing at the rods between the pores. The existence of cracks greatly affects the strength of structures. When external forces are applied, cracks quickly propagate and cause structural fracture. As the volume fraction of the lattice structure is greater than 40vol.%, the samples with neovius configuration show significant structural changes with closed pores and increased wall thickness. Closed pores can lead to residual slurry, resulting in differences between the designed porosity and the actual porosity.

No significant structural deformation is observed in the microstructure of the three configurations after sintering. Further, the linear shrinkage rates of Al_2O_3 ceramic micro lattice sintered bodies with three configurations at different volume fractions were measured in the length (x), width (y), and height (z) directions, as shown in Fig. 6. As can be seen in Fig. 6(a), the sample with gyroid configuration has the highest shrinkage in the height direction compared to length (x) and width (y) directions. The height (z) direction is the direction in which the 3D printed layers are stacked, and the bonding between the layers is weak, resulting in a large shrinkage. The sintering shrinkage in the length (x) and width (y) directions is similar, ensuring the shape accuracy of the sample with gyroid configuration in the printing plane. Figures 6(b) and (c) show the shrinkage rate changes of the samples with diamond and neovius configurations, respectively. The samples with these two configurations also have the highest shrinkage rate in the height direction, but the shrinkage rate in the width direction is greater than that in the length direction. The difference in shrinkage rate in three directions can cause slight deformation of the structure during sintering. Therefore, among the three lattice configurations, the gyroid configuration has the smallest deformation during sintering and exhibits higher dimensional accuracy.

Shrinkage is maximum in the height direction for all three configurations. Therefore, the shrinkage data in the height

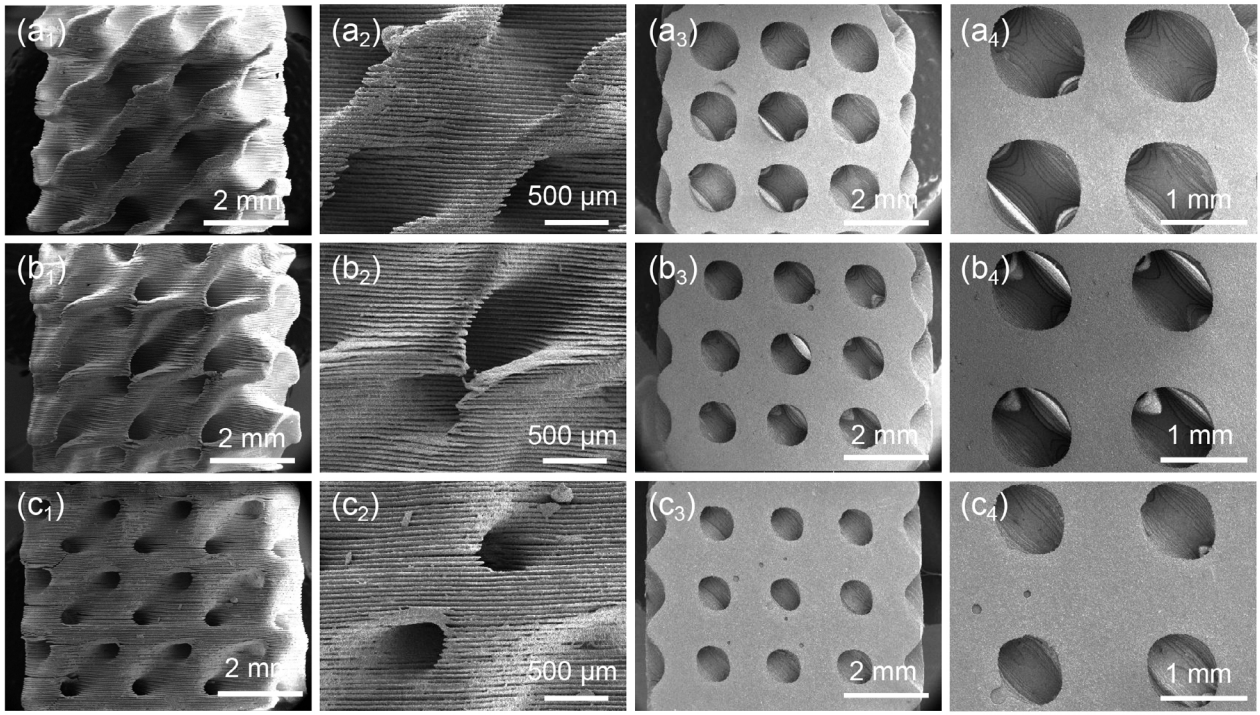

Fig. 4: SEM images of the Al_2O_3 ceramic micro lattice sintered bodies with diamond configuration: (a_1, a_2) the side surface of diamond-30; (a_3, a_4) the bottom surface of diamond-30; (b_1, b_2) the side surface of diamond-40; (b_3, b_4) the bottom surface of diamond-40; (c_1, c_2) the side surface of diamond-50; (c_3, c_4) the bottom surface of diamond-50

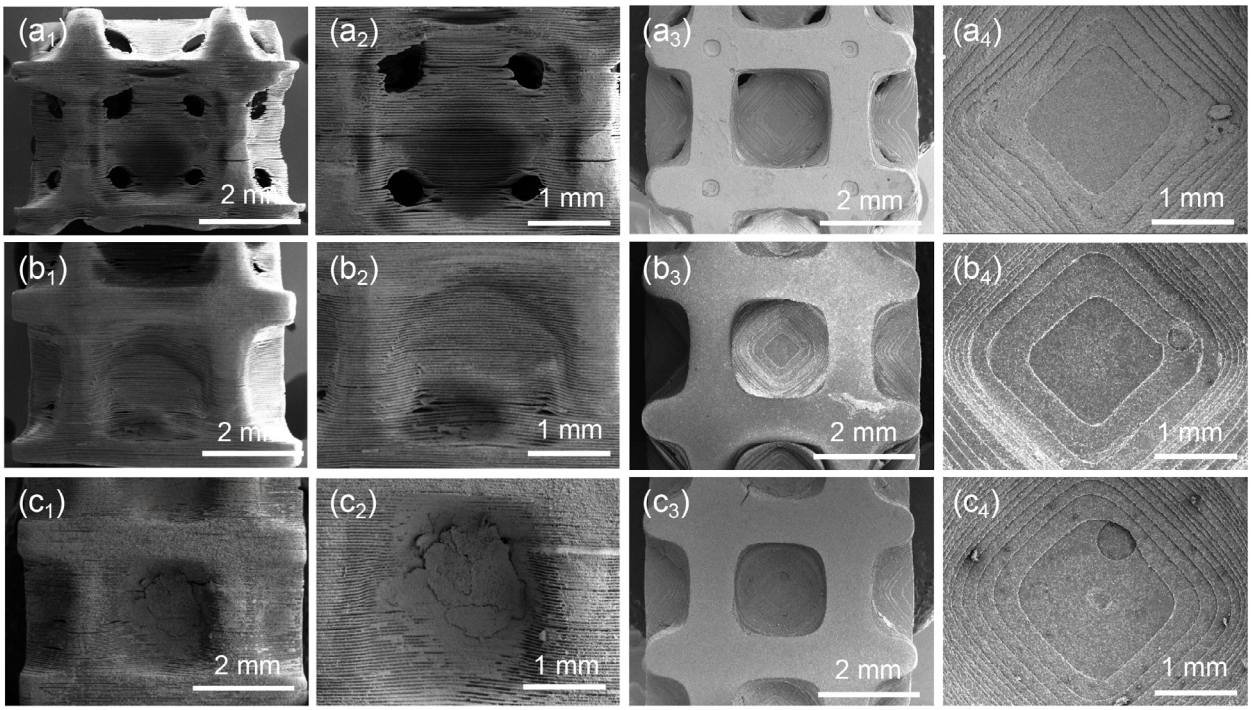

Fig. 5: SEM images of the Al_2O_3 ceramic micro lattice sintered bodies with neovious configuration: (a_1, a_2) the side surface of neovius-30; (a_3, a_4) the bottom surface of neovius-30; (b_1, b_2) the side surface of neovius-40; (b_3, b_4) the bottom surface of neovius-40; (c_1, c_2) the side surface of neovius-50; (c_3, c_4) the bottom surface of neovius-50

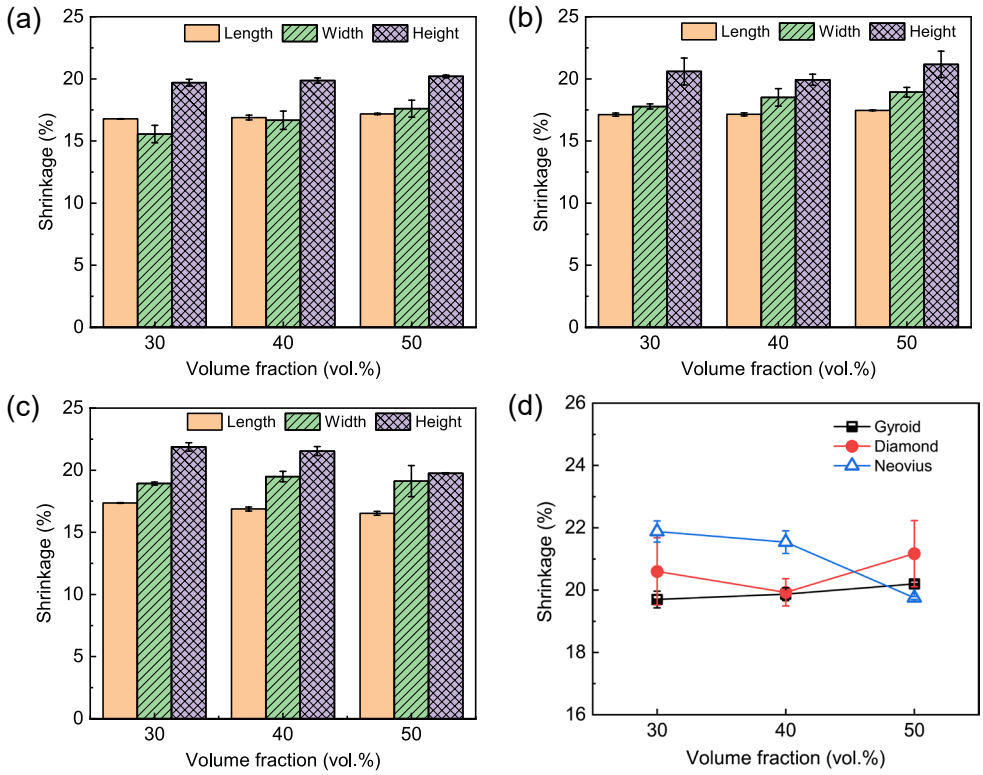

Fig. 6: Effects of structural configuration and volume fraction lattice structure on the shrinkage: (a) gyroid; (b) diamond; (c) neovius; (d) shrinkage in *z* direction

direction were used to analyze the trend of shrinkage as the volume fraction of the lattice structure, the results are shown in Fig. 6(d). As the volume fraction of the lattice structure increases, the sintering shrinkage of each configuration changes in a small scale, between 19% and 22%, indicating that the volume fraction of the lattice structure has little effect on the shrinkage of ceramic cores with TPMS structures. The shrinkage rates of the three configurations are similar, ranging from 19% to 22% overall. Take the shrinkage in *z* direction for comparison, when the volume fraction of the lattice structure is 30vol.%, the average linear shrinkage rates of the samples with gyroid, diamond, and neovius configurations

are 19.67%, 20.56%, and 21.86%, respectively. When the volume fraction of the lattice structure is 40vol.%, the average linear shrinkage rates of the samples with gyroid, diamond, and neovius configurations are 19.90%, 19.96%, and 21.51%, respectively. When the volume fraction of the lattice structure is 50vol.%, the average linear shrinkage rates of the samples with gyroid, diamond, and neovius configurations are 20.14%, 21.15%, and 19.73%, respectively. In short, the relationship between the shrinkage of the three lattice configurations is: neovius>diamond>gyroid. Based on the surface morphology of sintered ceramic cores, closed pores appear in the neovius configuration, and the shape of the concave part of the structure is blurred. After 3D printing, the residue of the slurry affects the shape accuracy and leads to abnormal changes in shrinkage rate for the samples with diamond configuration when the volume fraction of the lattice structure is 50vol.%, which should be discussed in deep in the future work.

3.2 Flexural strength

The samples with 6 mm×8 mm×40 mm for the flexural strength testing are shown in Fig. 7. Figure 8 shows the flexural strength of the Al_2O_3 ceramic micro lattice sintered bodies with different structural configurations and different volume fractions.

When the volume faction of the lattice structure is 50vol.%, the porosity is as high as 50%. The average flexural strength of the 3D printed Al_2O_3 ceramic micro lattice structures with gyroid, diamond, and neovius are 110.9, 139.1, and 81.1 MPa, respectively. When the volume faction of the lattice structure is 40vol.%, the porosity is as high as 60%. The average flexural strength of the 3D printed Al_2O_3 ceramic micro lattice structures

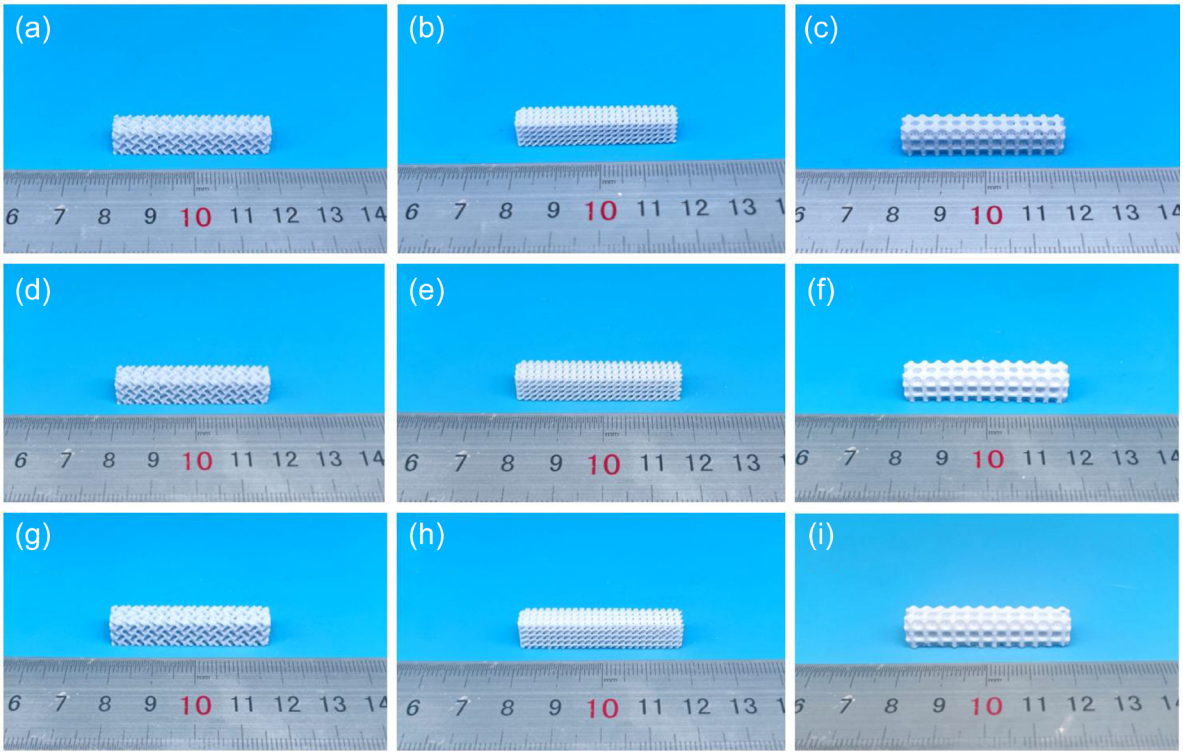

Fig. 7: Three-point flexural samples with micro lattice structures: (a) gyroid-30; (b) diamond-30; (c) neovius-30; (d) gyroid-40; (e) diamond-40; (f) neovius-40; (g) gyroid-50; (h) diamond-50; (i) neovius-50

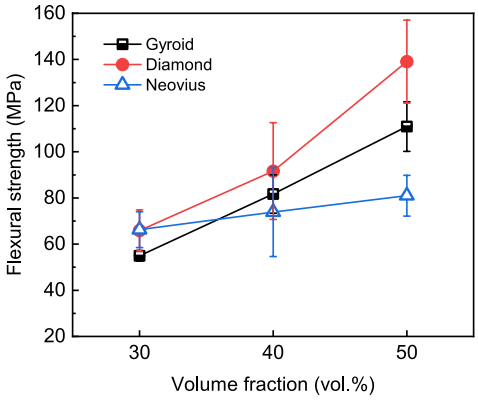

Fig. 8: Effects of structural configuratios and volume fractions of lattice structures on flexural strength of 3D printed Al_2O_3 ceramic micro lattice structures

with gyroid, diamond, and neovius are 80.8, 91.5, and 73.3 MPa, respectively. When the volume faction of the lattice structure is 30vol.%, the porosity is as high as 70%, which is the highest porosity value. At this time, the average flexural strength of the 3D printed Al_2O_3 ceramic micro lattice structures with gyroid, diamond, and neovius are 53.8, 66.1, and 66.4 MPa, respectively. Even when the volume fraction of the lattice structure is 30vol.%, that is to say the porosity is 70%, the flexural strength is as high as 50–70 MPa, which can still be maintained at a high level and is believed to be helpful for the following casting [10]. On the one hand, it is found that with the volume fraction of the 3D printed Al_2O_3 ceramic micro lattice structures increases, their flexural strength increases correspondingly. It can be seen from Figs. 3, 4, and 5 that

the pores of the Al_2O_3 ceramic micro lattice sintered bodies decrease and the wall thickness increases with the volume fraction of the lattice structure enhancement. The increase in wall thickness improves the structural stability and brings about an increase in the flexural strength of the core. On the other hand, when the volume fraction of the lattice structure is a certain value, the sample with diamond configuration has the highest strength, which may be attributed to it has the smoothest surface and transition zone, as shown in Fig. 4. It should be also noted that detailed stress analysis by simulation and experiments should be further conducted to reveal the mechanism for this phenomenon in future. The flexural strength of ceramic cores in current production applications is required to be greater than 30 MPa [7, 10], thus all these 3D printed Al_2O_3 ceramic micro lattice structures can meet the requirements for use. This indicates that the 3D printed Al_2O_3 ceramic micro lattice structures have great advantages for the performance improvement of ceramic cores, which can maintain high porosity and high strength simultaneously.

Figure 9 summaries the flexural strength and porosity data of different Al_2O_3 ceramic cores from existing studies [13-15, 17, 23-27]. The Al_2O_3 ceramic micro lattice structures prepared by 3D printing show a substantial improvement in porosity and flexural strength compared to conventional methods and other 3D printing methods. By 3D printing of these micro lattice structures, the internal porous structure of the core can be accurately controlled, achieving ordered pore formation. The prepared cores have excellent mechanical properties, providing a new way to further improve the performance of alumina ceramic cores.

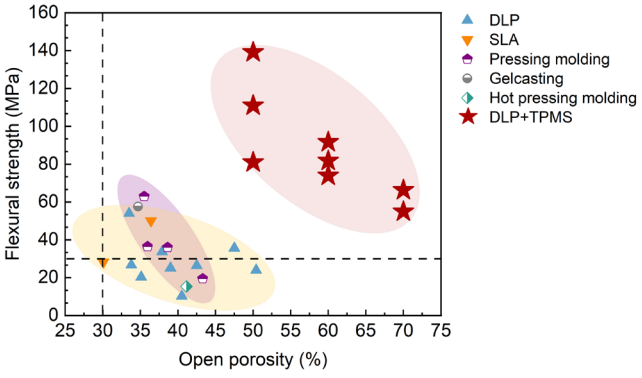

Fig. 9: Comparison of flexural strength and porosity of Al_2O_3 ceramic cores reported in the references (DLP+TPMS represents this work) [13-15, 17, 23-27]

3D printed micro lattice structure is applied to the field of ceramic core preparation to achieve precise control of the core structure and complete the leap from disordered to ordered pore making. However, the research scope of this study is limited by the experimental and testing conditions. In the future, the following prospects are proposed in the research of high-performance ceramic cores:

(1) As the key components of precision casting, ceramic cores usually work in a ultra-high temperature environment above 1,500 °C. And with the high temperature alloy casting temperature continues to rise, the ceramic core temperature capacity continues to pose a challenge. Therefore, in terms of performance testing, in addition to focusing on room temperature flexural strength, its high temperature performance should receive more attention.

(2) Ceramic cores in investment casting must withstand molten-metal impact, thermal shock, and solidification stresses. These conditions far beyond the scope of laboratory testing. During the actual production process, factors such as alloy chemistry, pouring dynamics, and cooling rates have a crucial impact on the performance of cores, making in-situ validation indispensable. Only by integrating the core into full-scale casting tests can its structural integrity, dimensional accuracy, and deformation resistance under operational loads be verified, thereby determining whether it meets the requirements for practical applications.

4 Conclusions

In this study, 3D printed micro lattice structures were innovatively applied to alumina ceramic cores. The effects of the three TPMS configurations (gyroid, diamond, and neovius) with different volume fractions (30%, 40%, and 50%) on the micro-morphology, shrinkage, and flexural strength of alumina ceramic cores were investigated. The following conclusions are drawn:

(1) There is a certain volume shrinkage during the sintering process of 3D printed micro lattice structures. The sintering shrinkage rate of the three configurations does not change significantly with increasing volume fraction of the lattice structure, and overall ranges from 19% to 22%. The relationship between the shrinkage rates of different configurations is neovius configuration>diamond configuration>gyroid configuration. For the same structure, shrinkage is highest in the height direction.

(2) As the volume fraction increases, all the three configurations show a decrease in pore size and an increase in wall thickness. The overall structure of the gyroid configuration is unchanged and the diamond configuration has an increased number of connected parts, but the pores of both structures are connected. The neovius configuration shows closed pores and more printing defects when volume fractions of lattice structures are greater than 40vol.%. Corresponding to the microstructure, the de-coring performance of the gyroid configuration and diamond configuration is similar and superior to that of the neovius configuration.

(3) When the volume faction of the lattice structure is 30vol.%, the porosity is as high as 70%, which is the highest porosity value in this study. At this time, the average flexural strength of the 3D printed Al_2O_3 ceramic micro lattice structures with gyroid, diamond, and neovius are 53.8, 66.1, and 66.4 MPa, respectively, which can still be maintained at a high level and is believed to be helpful for the following casting.

From this study, by using 3D printing the internal porous structure of the core with a micro lattice structure can be accurately controlled, achieving ordered pore formation. The prepared core has excellent mechanical properties, providing a new way to further improve the performance of ceramic cores.

Acknowledgments

This work was financially supported by the National Natural Science Foundation of China (Grant No. 52275310). The authors also want to sincerely thank the characterization at the Analysis & Testing Center, Beijing Institute of Technology.

Conflict of interest

The authors declare that they have no known competing financial interests or personal relationships that could have appeared to influence the work reported in this paper.

References

[1] Zheng W, Wu J M, Chen S, et al. Influence of Al_2O_3 content on mechanical properties of silica-based ceramic cores prepared by stereolithography. J. Adv. Ceram., 2021, 10(6): 1381–1388.
[2] Zhao G, Hu K H, Feng Q, et al. Creep mechanism of zircon-added silica ceramic cores formed by stereolithography. Ceram. Int., 2021, 47(12): 17719–17725.
[3] Hu K H, Wang H Y, Lu K, et al. Fabrication of silica-based ceramic cores with internal lattice structures by stereolithography. China Foundry, 2021, 19(5): 369–379.
[4] Li J G, An X L, Liang J J, et al. Recent advances in the stereolithographic three-dimensional printing of ceramic cores: Challenges and prospects. J. Mater. Sci. Technol., 2022, 117: 79–98.
[5] Wang X D, Mei X S, Wang X T, et al. Picosecond laser trimming of ceramic cores with porous multi-scale particle microstructure. Ceram. Int., 2021, 48(6): 7593–7604.
[6] Liu F C, Fan Z T, Liu X W, et al. Aqueous gel casting of water-soluble calcia-based ceramic core for investment casting using epoxy resin as a binder. Int. J. Adv. Manuf. Technol., 2016, 86: 1235–1242.
[7] Li Q L, Chen T C, Liang J J, et al. Manufacturing of ceramic cores: From hot injection to 3D printing. J. Mater. Sci. Technol., 2023, 134: 95–105.
[8] Fan J, Li Q L, Jin F N, et al. High solid loading, low viscosity stereolithography 3D printing ceramic cores slurry. Ceram. Int., 2023, 49(24): 40705–40715.
[9] Jin F N, Li Q L, Yang K, et al. Optimisation and application of high solid loading stereolithography 3D printing ceramic cores slurry. Ceram. Int., 2024, 50(2): 3574–3583.
[10] Zhai X F, Chen J Y, Zhang X Q, et al. Recent progresses and challenges of 3D printing of ceramic cores. J. Ceram., 2023, 44(5): 831–848.
[11] Zhang H, Lu Z, Ji Z, et al. Basis for the alkaline removal process design of the alumina-based ceramic core. J. Ceram. Soc. Jpn., 2017, 125(8): 616–622.
[12] Zhu W J, Tian G Q, Lu Y, et al. Leaching improvement of ceramic cores for hollow turbine blades based on additive manufacturing. Adv. Manuf., 2019, 7: 353–363.
[13] Li H, Liu Y S, Colombo P, et al. The influence of sintering procedure and porosity on the properties of 3D printed alumina ceramic cores. Ceram. Int., 2021, 47(19): 27668–27676.
[14] Li H, Liu Y S, Li W B, et al. The effect of sintering on the properties of calcium oxide promoted alumina-based ceramic cores via 3D printing. Mater. Chem. Phys., 2021, 263(4): 124443.
[15] Li H, Liu Y S, Liu Y S, et al. Influence of debinding holding time on mechanical properties of 3D-printed alumina ceramic cores. Ceram. Int., 2021, 47(4): 4884–4894.
[16] Zhai X F, Chen J Y, Wang Y R, et al. Fabrication of Al_2O_3 ceramic cores with high porosity and high strength by vat photopolymerization 3D printing and sacrificial templating. Ceram. Int., 2023, 49(19): 32096–32103.
[17] Li Q L, An X L, Liang J J, et al. Balancing flexural strength and porosity in DLP-3D printing Al_2O_3 cores for hollow turbine blades. J. Mater. Sci. Technol., 2022, 104: 19–32.
[18] Zhai X F, Chen J Y, Su R Y, et al. Vat photopolymerization 3D printing of Al_2O_3 ceramic cores with strip-shaped pores by using polyamide 6 fiber template. J. Am. Ceram. Soc., 2024, 107(8): 5400–5411.
[19] Wang Y J, Xu F, Gao H J, et al. Elastically isotropic truss-plate-hybrid hierarchical microlattices with enhanced modulus and strength. Small, 2023, 19(18): 2206024.
[20] Wang Y J, Zhang X, Li Z H, et al. Achieving the theoretical limit of strength in shell-based carbon nanolattices. PNAS, 2022, 119(34): e2119536119.
[21] Zhang W Q, Ye H T, Feng X B, et al. Tailoring mechanical properties of PμSL 3D-printed structures via size effect. Int. J. Extrem. Manuf., 2022, 4(4): 045201.
[22] Feng Y R, Guo X, Huang K, et al. Enhanced electromagnetic microwave absorption of SiOC ceramics targeting the integration of structure and function. J. Eur. Ceram. Soc., 2021, 41(13): 6393–6405.
[23] Tang W Z, Zhao T, Dou R, et al. Additive manufacturing of low-shrinkage alumina cores for single-crystal nickel-based superalloy turbine blade casting. Ceram. Int., 2022, 48(10): 15218–15226.
[24] Li H, Liu Y S, Liu Y S, et al. Influence of sintering temperature and CVI time on mechanical properties of 3D-printed alumina ceramics. Mater. Lett., 2021, 285(2): 129096.
[25] Li H, Liu Y S, Liu Y S, et al. Evolution of the microstructure and mechanical properties of stereolithography formed alumina cores sintered in vacuum. J. Eur. Ceram. Soc., 2020, 40(14): 4825–4836.
[26] Li H, Liu Y S, Liu Y S, et al. Silica strengthened alumina ceramic cores prepared by 3D printing. J. Eur. Ceram. Soc., 2021, 41(4): 2938–2947.
[27] Li X, Su H, Dong D, et al. Enhanced comprehensive properties of stereolithography 3D printed alumina ceramic cores with high porosities by a powder gradation design. J. Mater. Sci. Technol., 2022, 131: 264–275.